



UNIVERSITY OF LEEDS

This is a repository copy of *Experimental study of the deformation and breakage of 3D printed agglomerates: Effects of packing density and inter-particle bond strength*.

White Rose Research Online URL for this paper:  
<http://eprints.whiterose.ac.uk/137923/>

Version: Accepted Version

---

**Article:**

Ge, R, Ghadiri, M [orcid.org/0000-0003-0479-2845](https://orcid.org/0000-0003-0479-2845), Bonakdar, T et al. (3 more authors) (2018) Experimental study of the deformation and breakage of 3D printed agglomerates: Effects of packing density and inter-particle bond strength. Powder Technology, 340. pp. 299-310. ISSN 0032-5910

<https://doi.org/10.1016/j.powtec.2018.09.029>

---

© 2018 Elsevier B.V. All rights reserved. Licensed under the Creative Commons Attribution-Non Commercial No Derivatives 4.0 International License (<https://creativecommons.org/licenses/by-nc-nd/4.0/>).

**Reuse**

This article is distributed under the terms of the Creative Commons Attribution-NonCommercial-NoDerivs (CC BY-NC-ND) licence. This licence only allows you to download this work and share it with others as long as you credit the authors, but you can't change the article in any way or use it commercially. More information and the full terms of the licence here: <https://creativecommons.org/licenses/>

**Takedown**

If you consider content in White Rose Research Online to be in breach of UK law, please notify us by emailing [eprints@whiterose.ac.uk](mailto:eprints@whiterose.ac.uk) including the URL of the record and the reason for the withdrawal request.



[eprints@whiterose.ac.uk](mailto:eprints@whiterose.ac.uk)  
<https://eprints.whiterose.ac.uk/>

# **Experimental study of the deformation and breakage of 3D printed agglomerates: effects of packing density and inter-particle bond strength**

Ruihuan Ge<sup>1</sup>, Mojtaba Ghadiri<sup>2</sup>, Tina Bonakdar<sup>2</sup>, Zongyan Zhou<sup>3</sup>, Ian Larson<sup>4</sup> & Karen Hapgood<sup>1</sup>

1 Monash Advanced Particle Engineering Laboratory, Department of Chemical Engineering, Monash University, Clayton, Victoria 3800, Australia

2 Institute of Particle Science and Engineering, University of Leeds, UK

3 Laboratory for Simulation and Modeling of Particulate Systems, Department of Chemical Engineering, Monash University, Clayton, Victoria 3800, Australia

4 Drug Delivery, Disposition and Dynamics, Monash Institute of Pharmaceutical Sciences, Monash University, Parkville, Victoria 3052, Australia

E-mail: [karen.hapgood@deakin.edu.au](mailto:karen.hapgood@deakin.edu.au)

## **Abstract**

Characterisation of the mechanical properties of agglomerates is important in order to understand their deformation and breakage. However, research progress has been hampered by limitations in our ability to manufacture reproducible agglomerates with well-controlled and fully characterised mechanical properties. In this paper, we report on the preparation and testing of agglomerates with tuneable properties using 3D printing technology. Two typical agglomerate structures with different packing densities were designed and printed using a PolyJet 3D printer. Each agglomerate consisted of rigid primary particles connected by either rigid or rubber-like inter-particle cylindrical bonds. Compression tests (using speeds in the range 0.02 -0.5 mm/s) and drop weight impact tests were carried out to investigate the effect of bond material and strain rate on mechanical properties of the agglomerates. The results show that strain rate affects their deformation and breakage significantly, and breakage patterns of the two structures are different under uniaxial compression and impact test conditions. These results demonstrate the broad utility of 3D printed agglomerates as ideal “test” agglomerates for a range of breakage studies, including validating computer simulations of DEM breakage.

**Keywords:** 3D printing; Agglomerates; Breakage test; Strain rate

## 1. Introduction

Particulate solids in agglomerate form are widely used in chemical, pharmaceutical and food industry. Typical agglomerates have complex porous structures, in which small primary particles are bonded together by adhesive forces or by binding materials [1]. The mechanical strength of agglomerates plays an important role during handling, storing and transportation. However, due to their complex internal structures and inhomogeneous composition, there is still no reliable predictive method that can describe the strength and breakage behaviour of agglomerates.

In general, the mechanical properties of single agglomerates can be experimentally examined under well-defined stress conditions. Quasi-static compression test and impact test under high strain rates are commonly used methods to investigate the agglomerate breakage characteristics. Many experimental studies considering various agglomerate materials and test conditions have been reported previously. Table 1 lists a few examples of experimental breakage studies of a single dry agglomerate under quasi-static compression, while Table 2 summarises some examples of impact breakage studies. The mechanical responses of agglomerates vary from brittle and semi-brittle to plastic depending on their constitutions and loading conditions. Overall, agglomerate deformation and breakage is complex and can be influenced by multiple parameters including structure, loading rate and bonding mechanisms.

<Table 1. Agglomerate breakage studies using quasi-static compression test [2-9]>

<Table 2. Agglomerate breakage studies using impact test [10-16]>

The main challenge of agglomerate breakage research is that each individual agglomerate tested has a unique structure and therefore unique breakage behaviour. However breakage tests are destructive and can only be performed on each single sample at one set condition, and cannot be repeated or varied under different conditions. Thus experimental breakage data have a large scatter, as a result of the unrepeatability of the tests due to the unique structure of the

agglomerates. It is necessary to offer a way to produce model agglomerates with desired properties. Antonyuk et al. [6, 17] studied the compression breakage mechanisms of three model spherical granules i.e.  $\gamma$ -Al<sub>2</sub>O<sub>3</sub>, zeolite and sodium benzoate, with their mechanical characteristics ranging from elastic to plastic. Breakage results were obtained and analysed using force-displacement curves and continuum contact mechanics models. In addition, they prepared cylindrical agglomerates by compressing spherical alumina particles in a die, and investigated the effect of binder content and agglomerate size on the agglomerate strength. Subero et al. [11] studied the impact breakage of agglomerates using moulded agglomerates with defined structures and bond properties. Different breakage patterns of agglomerates have been reported in their work, and the results mainly show that the dominant breakage pattern changes from localised damage to multiple fragmentations with increased impact velocities and solid fractions. The main limitation of previous work is that model agglomerates that precisely replicate the inhomogeneity of agglomerate structure can be difficult to make. X-ray micro-tomography is now available to obtain the agglomerate structural details [18, 19]. Golchert et al. [18] were the first to study the compressive breakage of agglomerates with 3D spatial locations of particles fully characterised by X-ray micro-tomography. However, control of agglomerate structure and mechanical properties for producing replicate agglomerates is still difficult, unless a new method to produce model agglomerate is applied. One aim of this work is to provide a way by 3D printing to precisely control the agglomerate structure and inter-particle bond properties to systematically investigate their influence on the agglomerate strength.

Another aim is to provide reproducible structures that can be rigorously analysed by simulations. Nowadays Discrete Element Method (DEM) simulations are used along with experimental work, as it offers an easy way to understand the effects of different parameters on the agglomerate strength. A large number of parameters influencing agglomerate breakage, e.g. structure details, interface energy, and shapes have been examined using DEM [18-20]. However, most simulations use average mechanical and structure parameters that eliminate the complexity of real agglomerates at the very beginning. Thus the simulation results cannot accurately predict the properties of single agglomerates, especially for those bonded by binders. It is necessary to offer an experimental method to provide a basis for the improvement and validation of DEM models.

In our research, PolyJet 3D printing technology is used to produce model agglomerates. This technology has a printing resolution of 16-30  $\mu\text{m}$  layer thickness, and can simultaneously print multiple materials with varying mechanical properties ranging from rigid to ductile behaviour. Previously, a symmetrical agglomerate with a simple cubic structure was designed and printed to demonstrate the feasibility of this method on agglomerate breakage research [21]. In this work, a series of agglomerate deformation and breakage tests have been carried out with controlled variations. Two different spherical agglomerates with random internal structures are designed and printed. These random structures are one step closer to real agglomerates compared to the symmetrical structure tested in the previous work. Both the primary particle and inter-particle bond materials are well characterised. Compression and impact tests have been performed to investigate the deformation and breakage of these agglomerates under different loading rates.

## **2. Experimental method**

### **2.1 Agglomerate design**

Two different agglomerate structures were designed as shown in Figure 1. Each structure had 120 primary particles connected together by cylindrical inter-particle bonds. Primary particle positions were randomly generated in a spherical volume using the “particle factory” function in EDEM software (DEM Solutions, Edinburgh). Both agglomerates had a random structure and the porosity was varied by adjusting the average bond length to create a densely packed structure with a porosity of  $\varepsilon=44\%$  and a loosely packed structure with  $\varepsilon=57\%$ . For the dense structure ( $\varepsilon=44\%$ ), 120 particles were generated and assembled in a 25 mm diameter spherical space using  $10\text{ J/m}^2$  adhesion force. After generating the dense structure, the spherical geometry and adhesion force were set to zero, so that the primary particles moved away from each other until expanding to a 30 mm diameter spherical space, by which a loosely packed structure ( $\varepsilon=57\%$ ) was obtained.

For the dense agglomerate structure, the primary particles within 4.3 mm of each other (center to center distance) are considered to be joined by a 2 mm diameter bond. The average coordination number of the dense structure is  $\text{CN}=4.1$ . For the loose agglomerate structure, a 5.6 mm center to center connect distance is chosen. The corresponding average coordination number of the loose structure is  $\text{CN}=4.9$ . The doublet dimension including particle and bond

size is shown in Figure 2. The volume fractions of bond, particle and air in these two structures are given in Figure 3.

<Figure 1. Agglomerate structures (Left: front view Right: cross-sectional view)>

<Figure 2. Schematic of a single doublet, the centre to centre distance between the particles varies based on the agglomerate design and for each particle.>

<Figure 3. Phase volume fractions in two different agglomerate structures. >

Details of the agglomerate design and production process are illustrated in Figure 4. The generated particle positions were exported into Solidworks software. In Solidworks, the agglomerate structures were replicated and discrete particles were connected by cylindrical bonds. The white particles and the black inter particle bonds were defined as separate objects and can be printed using different 3D printing materials. The agglomerate designs were then converted to STL format files and imported into Objet 500 3D printer as a 3D printing task. Detailed printing and support removal processes have been reported previously [21]. The Objet 3D printer uses PolyJet technology that can simultaneously print multiple materials with varied mechanical properties. In this work, the primary particles were printed using rigid VeroWhitePlus™ and the bonds were printed using either the same rigid VeroWhitePlus™ (i.e. the entire agglomerate is printed from a single material) or the rubber-like DM 9895 [22]. Considering the two different agglomerate structures and two different bond materials, there were in total four different agglomerate types used in this work. Descriptions of each agglomerate are summarised in Table 3.

<Figure 4. Agglomerate design and production process>

<Table 3. Summary of four agglomerate types used in this research>

## 2.2 Experimental setup

Compression and drop weight impact tests were carried out to analyse the mechanical characteristics of agglomerates at different strain rates. Tests were conducted on the

agglomerates, and also on small cylindrical samples (10 mm high and 10 mm diameter) of the two polymers (VeroWhitePlus™ and DM 9895). A schematic diagram of the test setup is illustrated in Figure 5.

Compression tests were conducted using an Instron 5566 universal testing machine with a 10 kN load cell and the breakage progress was filmed using a Nikon D7000 camera. As shown in Figure 5 (a-b), agglomerates or polymer cylinders were compressed between two metal plates at three different cross-head loading speeds of 0.02 mm/s, 0.1 mm/s and 0.5 mm/s. The compressive load applied by the upper plate was recorded and analysed. Different loading modes including monotonic loading and cyclic loading were considered in this study. For the cyclic loading tests on agglomerates, the loading and unloading tests were repeated with a sequence of increased displacement, i.e. 0.5 mm, 1 mm, 2 mm and 4 mm. Additionally, each agglomerate type was subjected to 20 compression cycles under 0.1 mm/s loading rate. For the dense structured and loose structured agglomerates, the maximum compression displacement was 2 mm and 4 mm, respectively.

Drop weight impact tests were performed to analyse the impact deformation and breakage behaviour of agglomerates at high strain rates. As shown in Figure 5 (c), the impact test was conducted by placing the agglomerate sample on a flat anvil and dropping a cylindrical weight onto the sample from a 0.5 m height via a guide tube. For the agglomerates with dense structure, a 0.2 kg weight impactor (0.9 J impact energy) was used. For the agglomerate with loose structure, a 0.6 kg weight impactor (2.7 J impact energy) was also used as the former did not fracture the whole structure. For all the impact tests, the agglomerate orientation was kept the same with corresponding compression tests. The tests were video recorded using a high speed camera with a 5000 frames per second (f/s) sampling rate.

Previous research showed that the direction of 3D printing layers of objects with regard to the load direction influenced the results [21]. In this work, to ensure the same experimental conditions, the printed layers of all the test samples were kept horizontal (i.e. parallel to the test platen) for testing (See Figure 5). At least three replicates were performed for every experimental case to check the repeatability of the experiments.

<Figure 5. Schematic of breakage test setup>

### 3. Experimental results and analysis

#### 3.1 Mechanical properties of 3D printed materials

The stress-strain curves for uniaxial compression of 10 mm cylinders of the two main polymers used in this study are shown in Figures 6 and 7. The test conditions and cylindrical geometry are illustrated in the upper left of each figure. The light coloured cylinders represent rigid Vero WhitePlus™, while the dark grey coloured cylinders represent soft DM 9895 material. The experimental results show strain rate sensitivity and inelastic effects. Similar characteristics of polymer materials have been studied in previous works [23, 24]. The stress-strain curves of the rigid material (Vero WhitePlus™) show typical mechanical properties of a glassy polymer, i.e. rate-dependent elastic-plastic deformation. Initial linear elastic deformation, yielding, post-yield and strain softening can be distinguished from the curves (see Figure 6 (a)). The stress-strain curves of the soft material (DM 9895) show non-linear elastomeric behaviour (see Figure 6 (b)). As shown in Figure 7, both materials show inelastic behaviour during cyclic loading at  $0.002 \text{ s}^{-1}$ , which indicates energy dissipation. In particular, for the soft DM 9895 polymer, the initial loading cycle indicates a rubber-like behaviour. The amount of dissipated energy the rubber-like material dissipates is much higher if compared to the rigid material and this is evidenced by the slopes of the loading and unloading curves, which results in a more pronounced generated area.

Detailed mechanical properties of the rigid and soft 3D printing materials are listed in Table 4 and Table 5, respectively. As the soft material shows hyper-elastic behaviour, its nominal Young's modulus value is calculated as a function of strain for the initial linear region (below 20 % strain). For the rigid material, the failure strength corresponds to the appearance of plastic yielding, and for the soft material, the failure strength means the material collapses by fracture. As shown in Tables 4-5, for both materials, Young's modulus and compressive strength increase with increased strain rates.

<Figure 6. Uniaxial compression curves of 3D printing materials>

<Figure 7. Cyclic loading test results of 3D printing materials ( $0.002 \text{ s}^{-1}$  strain rate)>

<Table 4. Mechanical properties of rigid 3D printing materials (Vero WhitePlus™) under uniaxial compression tests, as a function of strain rate>

<Table 5. Mechanical properties of soft 3D printing materials (DM 9895) under uniaxial compression tests, as a function of strain rate>

### 3.2 Agglomerate deformation and breakage under compression

Typical compressive breakage curves for those four agglomerate types in Table 3 are shown in Figures 8 to 11. The load-displacement curves are obtained using uniaxial compression tests with a 0.02 mm/s displacement controlled loading rate. For each figure, a corresponding load-unload curve is shown in the inset to reveal the elastic-plastic deformation of agglomerates. For the same agglomerate types, the breakage results show good reproducibility. However, the load-displacement curves show different behaviours for different agglomerate structures and bond materials.

Figure 8 illustrates the deformation and breakage process of the agglomerate with dense structure and rigid bond. At a low displacement, the agglomerate mainly shows elastic-plastic deformation. The load increases with displacement and reaches the peak value at around 4 mm displacement which corresponds to the breakage point. At this point, the agglomerate breaks into two main fragments through the meridian plane. As illustrated in Figure 9, a similar breakage process is observed for the agglomerate with the same structure and soft bond material. The load-displacement curves show a clear drop at around 2.5 mm displacement accompanied by the appearance of a meridian crack.

Figure 10 illustrates the deformation and breakage process of the agglomerate with the loose structure and rigid bond. The load-displacement curves can be divided into several stages. At a low displacement, the structure deforms in a linear way and the curves mainly show elastic-plastic deformation. At around 2 mm displacement, the curves level off, giving the appearance of yielding behaviour which corresponds to the reconfiguration of particles and porosities inside the structure. After the yielding stage, the test samples show a hardening response. The agglomerate deforms plastically until 7 mm displacement, when the load drops indicating the occurrence of breakage. Figure 11 shows the agglomerate deformation and breakage with the

same loose structure and soft bond material. The curves show elastic-plastic deformation at the initial stage. After 6 mm displacement, breakage and ductile failure behaviour can be observed from the curves. For both agglomerates with loose structure, the breakage occurs at a larger deformation compared with the dense structured agglomerate, and the agglomerate structure is crushed progressively without a clear fracture plane (see camera stills in Figures 10 and 11).

The comparisons of force-displacement curves of agglomerates under different loading rates are shown in Figure 12. For all agglomerate types, at the initial loading stage before breakage point, the compressive load increases with increasing loading rate. For the agglomerates with rigid bond materials, at higher loading rates (0.1 mm/s and 0.5 mm/s), the compressive loads show semi-brittle breakage characteristics (see Figures 12 a and c). However, for the agglomerates with soft bond materials, the deformation and breakage curves all show ductile failure, and the failure strength increases with increased loading rates (see Figures 12 b and d).

Overall, the compression test results show that the agglomerate with dense structure breaks through the meridian plane. By contrast, the agglomerate with loose structure deforms progressively and breaks without clear fracture plane. The compressive load responses are different in terms of different bond materials. Under low strain rate, they show ductile failure behaviours. With increasing strain rate, the agglomerate structures with rigid bond materials show semi-brittle breakage characteristics. To further evaluate the effect of bond material properties, cyclic loading tests were conducted and presented in the next section.

<Figure 8. Force-displacement curves for the agglomerate with dense structure and rigid bond material under 0.02 mm/s loading condition (three replicates were performed, and a cyclic loading curve is shown in the inset)>

<Figure 9. Force-displacement curves for the agglomerate with dense structure and soft bond material under 0.02 mm/s loading condition (three replicates were performed, and a cyclic loading curve is shown in the inset)>

<Figure 10. Force-displacement curves for the agglomerate with loose structure and rigid bond material under 0.02 mm/s loading condition (three replicates were performed, and a cyclic loading curve is shown in the inset)>

<Figure 11. Force-displacement curves for the agglomerate with loose structure and soft bond material under 0.02 mm/s loading condition (three replicates were performed, and a cyclic loading curve is shown in the inset)>

<Figure 12. Force-displacement curves of various agglomerates under different loading conditions>

### 3.3 Cyclic loading compression tests

Cyclic loading tests under different loading rates have been performed to examine the energy dissipation and fatigue effects. As shown in Figure 13, all the tested agglomerates are loaded to a certain strain and unloaded. The loading and unloading tests are repeated on the same agglomerate with a sequence of increased displacement, i.e. 0.5 mm, 1 mm, 2 mm and 4 mm. As expected, for all the agglomerate types, the loading curves show strain rate sensitivity and hysteresis effects.

For the agglomerates with dense structure, the load-unload curves show similar variation trends under different stages (See Figures 13 a and b). However, for the agglomerates with loose structure, the characteristic shapes of load-unload cycles are different in terms of different bonding materials (see Figures 13 c and d). For the agglomerate with loose structure and rigid bond material, the curves show linear deformation at the initial displacement, which has a small dependence on the strain rate. After 2 mm displacement, strain softening effects occur, and the unloading curves show a significant amount of permanent plastic deformation at 4 mm displacement (see Figure 13 c). By contrast, the load-unload cycles of loose structured agglomerate with soft bond material show an apparent strain rate dependence at the very beginning stage and the compressive loads increase without strain softening effects (see Figure 13 d).

<Figure 13. Compressive curves during loading-unloading cycles in sequence of increasing displacements>

The load-unload loops in the curves of Figure 13 indicate the existence of energy dissipations during load-unload tests. Energy dissipation is depicted in Figure 14, where the dissipated energy  $W_{dis}$  is represented by the grey area, and the total energy  $W_T$  is given by the hatched area under the loading curve. Using numerical integration method, the dissipated energy is calculated and shown in Figure 15. For all cases, the energy dissipation increases with increased displacement. At a high displacement, the curves show strong strain rate dependency. In particular, Figure 15 c shows the relatively large dissipation energy of ~3500-4500 mJ at 4 mm displacement for the loose structured agglomerate with rigid bonds, which can be attributed to the onset of yielding behaviour.

To further characterise the energy dissipation effects, the agglomerates are repeatedly loaded up to a certain displacement, and then completely unloaded. As shown in Figure 16, each agglomerate type is subjected to 20 compression cycles under 0.1 mm/s loading rate. The maximum compression displacement was 2 mm and 4 mm, for the dense structured and loose structured agglomerates, respectively. From the load-unloading cycles in Figure 16, each loading cycle leads to a permanent residual deformation. This is larger for the rigid material bonded agglomerate than that of the soft material bonded agglomerate. The energy loss coefficient  $\eta$  is defined as follows [17]:

$$\eta = \frac{W_{dis}}{W_T} \quad (1)$$

The calculated energy loss coefficients  $\varepsilon$  for all the agglomerate types based on the results of Figure 16 are shown in Figure 17. The results indicate that with the increasing number of loading cycles, the energy loss coefficients of rigid bond agglomerate decreases and reaches an asymptotic value. The asymptotic values for the dense structure and loose structure are 0.3 and 0.5, respectively. In contrast, for the agglomerate with soft bonds, the energy loss coefficient shows a notable decrease in the first cycle and remains fairly constant afterwards. For both structures, the asymptotic value of the energy loss coefficients for the agglomerates with soft bonds are larger than those for the rigid bond agglomerates. This difference is attributed to the different mechanical properties of these two bond materials, which is consistent with the characterization of single materials (refer to Figure 7). Specifically, the rigid bond material shows elastic-plastic behaviour since the energy dissipation mainly occurs

during the permanent plastic flow (refer to Figure 7 a). In contrast, the soft bond shows viscous-elastic damping effects under the initial load-unload cycles (refer to Figure 7 b).

<Figure 14. Schematic of dissipated energy>

<Figure 15. Dissipated energy during cyclic loadings (the same tests as of Figure 13).>

<Figure 16. Compressive curves of 20 loading-unloading cycles under 0.1 mm/s loading rate>

<Figure 17. Energy loss coefficients of 20 loading-unloading cycles under 0.1 mm/s loading rate (the same tests as of Figure 16) >

### 3.4 Drop weight impact test

Figure 18 shows that the agglomerates with rigid bonds show semi-brittle breakage characteristics, and the breakage patterns differ for each structure. For the dense structured agglomerate, the agglomerate fails into two main fragments along the meridian crack plane. Similar impact breakage results have been reported in previous DEM simulation research [18, 19]. For the loose structured agglomerate, cracks initially occur near the impact site and then they expand to the whole structure. The loose agglomerate breaks into several fragments under 2.7 J impact energy (Figure 18 c). A possible explanation for the different breakage patterns is that for the dense structure, due to the compactness of primary particles, a strong force transmission chain can be easily formed and propagate into the whole structure across the meridian plane. However, for the loose structure, the impact force dissipates at the impact site, and fracture occurs along different pathways of the bond network [18].

The impact test results of agglomerates with soft bond material are shown in Figure 19. For all cases tested, the agglomerate sustains a high elastic deformation and then rebounds from the anvil without breakage. The rebound behaviour is attributed to the energy storage effects of soft bond material. The repeated compression results on DM 9895 materials (refer to Figure 7) showed that the elastic behaviour and the recovery capability of soft bond material is far higher

than that of rigid bond material. The existence of soft bond materials provides damage tolerance for the whole agglomerate structure.

<Figure 18. High speed camera recordings of impact test-rigid material bonded agglomerate>

<Figure 19. High speed camera recordings of impact test-soft material bonded agglomerate>

### 3.5 Discussion and outlook

Agglomerate properties including its deformation and breakage characteristics are difficult to be modelled and predicted. 3D printing offers a way to synthesize “ideal” agglomerates with controlled mechanical properties. Following on our previous “proof of concept” research, here we significantly expanded the testing types to increase the agglomerate complexity to demonstrate sorts of deformation and breakage behaviours. A range of mechanical properties have been explored considering variations in particle size, inter-particle bonds, internal porosities, multiple materials (for primary particles and bonds), strain rates, and different types of fracture mechanics (e.g. semi-brittle, elastic, plastic). In terms of application, this analogous particulate system can be used in same test equipment as real agglomerates to validate breakage models of particulate solids. Originally, DEM simulation combined with bond particle model is expected to simulate all this data of agglomerate breakage [25, 26] . However, current bond models are not sophisticated enough to capture various breakage characteristics under different strain rates shown in experiments. In addition, modelling of non-linear deformation behaviour and energy absorption effects under high strain rates is another issue that needs to be addressed.

## 4. Conclusions

In this paper, 3D printing was used to produce model agglomerates with reproducible structures. Random structured spherical agglomerates at two different porosities ( $\varepsilon = 44\%$  and  $\varepsilon = 57\%$ ) and two different bond strengths were designed and produced. For the first time, a series of macroscopic agglomerate breakage tests were carried out with well-defined microscopic particle and bond properties. The results show that the agglomerate structure, bond material and strain rates affect the agglomerate deformation and breakage mechanisms in different ways.

The experimental results show significant strain rate effects. For the rigid bonded agglomerates, they show ductile failure under a 0.02 mm/s loading rate, and the failure mode changes to semi-brittle fashion with increased loading rates. For the soft bonded agglomerates, they show ductile failure under compression test, and rebound behaviours under impact that arising from viscous damping of bond materials. Two agglomerate structures (i.e. dense structure and loose structure) show different breakage patterns. The dense structured agglomerates show clear meridian crack planes, while the loose structured agglomerates fail progressively from contact regions. Overall the breakage data produced demonstrates that the 3D printed agglomerates are suitable for use in a range of different tests, and are able to be used to demonstrate many different types of deformation, breakage and failure modes. The success of these demonstrations opens the door to reproducible data for future modelling of deformation and breakage, and offer a basis for developing more refined models on simulating agglomerate breakage under different strain rates, especially for agglomerates bonded by polymeric binders.

### **Acknowledgements**

This research project was supported by International Fine Particle Research Institute (IFPRI) and an ARC Discovery grant (DP150100119). Ruihuan Ge's PhD scholarship was supported by the China Scholarship Council (CSC). The authors would also like to acknowledge Dr. Alejandro López at University of Leeds for his comments on the paper draft.

### **References**

- [1] H. Rumpf, The strength of granules and agglomerate, *Agglomeration*, Interscience, New York, 1962, pp. 379-418.
- [2] H. Meissner, A. Michaels, R. Kaiser, Crushing strength of zinc oxide agglomerates, *Industrial & Engineering Chemistry Process Design and Development*, 3 (1964) 202-205.
- [3] W.J. Beekman, G.M.H. Meesters, T. Becker, A. Gaertner, M. Gebert, B. Scarlett, Failure mechanism determination for industrial granules using a repeated compression test, *Powder Technology*, 130 (2003) 367-376.
- [4] Y. Sheng, B.J. Briscoe, R. Maung, C. Rovea, Compression of polymer bound alumina agglomerates at the micro deformation scale, *Powder Technology*, 140 (2004) 228-239.

- [5] A. Samimi, A. Hassanpour, M. Ghadiri, Single and bulk compressions of soft granules: Experimental study and DEM evaluation, *Chemical Engineering Science*, 60 (2005) 3993-4004.
- [6] S. Antonyuk, J. Tomas, S. Heinrich, L. Mörl, Breakage behaviour of spherical granulates by compression, *Chemical Engineering Science*, 60 (2005) 4031-4044.
- [7] Y.S. Cheong, M.J. Adams, A.F. Routh, M.J. Hounslow, A.D. Salman, The production of binderless granules and their mechanical characteristics, *Chemical Engineering Science*, 60 (2005) 4045-4053.
- [8] S. Adi, H. Adi, H.-K. Chan, W.H. Finlay, Z. Tong, R. Yang, A. Yu, Agglomerate strength and dispersion of pharmaceutical powders, *Journal of Aerosol Science*, 42 (2011) 285-294.
- [9] A. Russell, P. Müller, H. Shi, J. Tomas, Influences of loading rate and preloading on the mechanical properties of dry elasto-plastic granules under compression, *AIChE Journal*, 60 (2014) 4037-4050.
- [10] Z. Ning, R. Boerefijn, M. Ghadiri, C. Thornton, Distinct element simulation of impact breakage of lactose agglomerates, *Advanced Powder Technology*, 8 (1997) 15-37.
- [11] J. Subero, M. Ghadiri, Breakage patterns of agglomerates, *Powder Technology*, 120 (2001) 232-243.
- [12] A. Samimi, M. Ghadiri, R. Boerefijn, A. Groot, R. Kohlus, Effect of structural characteristics on impact breakage of agglomerates, *Powder Technology*, 130 (2003) 428-435.
- [13] A. Samimi, R. Moreno, M. Ghadiri, Analysis of impact damage of agglomerates: effect of impact angle, *Powder Technology*, 143-144 (2004) 97-109.
- [14] A.D. Salman, G.K. Reynolds, J.S. Fu, Y.S. Cheong, C.A. Biggs, M.J. Adams, D.A. Gorham, J. Lukenics, M.J. Hounslow, Descriptive classification of the impact failure modes of spherical particles, *Powder Technology*, 143-144 (2004) 19-30.
- [15] S. Antonyuk, M. Khanal, J. Tomas, S. Heinrich, L. Mörl, Impact breakage of spherical granules: Experimental study and DEM simulation, *Chemical Engineering and Processing: Process Intensification*, 45 (2006) 838-856.
- [16] M. Khanal, W. Schubert, J. Tomas, Compression and impact loading experiments of high strength spherical composites, *International Journal of Mineral Processing*, 86 (2008) 104-113.
- [17] S. Antonyuk, S. Heinrich, J. Tomas, N.G. Deen, M.S. van Buijtenen, J.A.M. Kuipers, Energy absorption during compression and impact of dry elastic-plastic spherical granules, *Granular Matter*, 12 (2010) 15-47.

- [18] C. Thornton, L. Liu, How do agglomerates break?, Powder Technology, 143-144 (2004) 110-116.
- [19] L. Liu, K.D. Kafui, C. Thornton, Impact breakage of spherical, cuboidal and cylindrical agglomerates, Powder Technology, 199 (2010) 189-196.
- [20] D. Golchert, R. Moreno, M. Ghadiri, J. Litster, Effect of granule morphology on breakage behaviour during compression, Powder Technology, 143-144 (2004) 84-96.
- [21] R. Ge, M. Ghadiri, T. Bonakdar, K. Hapgood, 3D printed agglomerates for granule breakage tests, Powder Technology, (2016).
- [22] PolyJet Materials, pp. available online at <http://www.stratasys.com/materials/polyjet>.
- [23] J. Bergström, M. Boyce, Constitutive modeling of the large strain time-dependent behavior of elastomers, Journal of the Mechanics and Physics of Solids, 46 (1998) 931-954.
- [24] A.D. Mulliken, M.C. Boyce, Mechanics of the rate-dependent elastic–plastic deformation of glassy polymers from low to high strain rates, International Journal of Solids and Structures, 43 (2006) 1331-1356.
- [25] N.J. Brown, J.-F. Chen, J.Y. Ooi, A bond model for DEM simulation of cementitious materials and deformable structures, Granular Matter, 16 (2014) 299-311.
- [26] D.O. Potyondy, P.A. Cundall, A bonded-particle model for rock, International Journal of Rock Mechanics and Mining Sciences, 41 (2004) 1329-1364.

## Figures:

Figure 1. Agglomerate structures (Left: front view Right: cross-sectional view).

Figure 2. Schematic of a single doublet, the centre to centre distance between the particles varies based on the agglomerate design and for each particle.

Figure 3. Phase volume fractions in two different agglomerate structures.

Figure 4. Agglomerate design and production process.

Figure 5. Schematic of breakage test setup.

Figure 6. Uniaxial compression curves of 3D printing materials.

Figure 7. Cyclic loading test results of 3D printing materials ( $0.002 \text{ s}^{-1}$  strain rate).

Figure 8. Force-displacement curves for the agglomerate with dense structure and rigid bond material under  $0.02 \text{ mm/s}$  loading condition (three replicates were performed, and a cyclic loading curve is shown in the inset).

Figure 9. Force-displacement curves for the agglomerate with dense structure and soft bond material under  $0.02 \text{ mm/s}$  loading condition (three replicates were performed, and a cyclic loading curve is shown in the inset).

Figure 10. Force-displacement curves for the agglomerate with loose structure and rigid bond material under  $0.02 \text{ mm/s}$  loading condition (three replicates were performed, and a cyclic loading curve is shown in the inset).

Figure 11. Force-displacement curves for the agglomerate with loose structure and soft bond material under  $0.02 \text{ mm/s}$  loading condition (three replicates were performed, and a cyclic loading curve is shown in the inset).

Figure 12. Force-displacement curves of various agglomerates under different loading conditions.

Figure 13. Compressive curves during loading-unloading cycles in sequence of increasing displacements.

Figure 14. Schematic of dissipated energy.

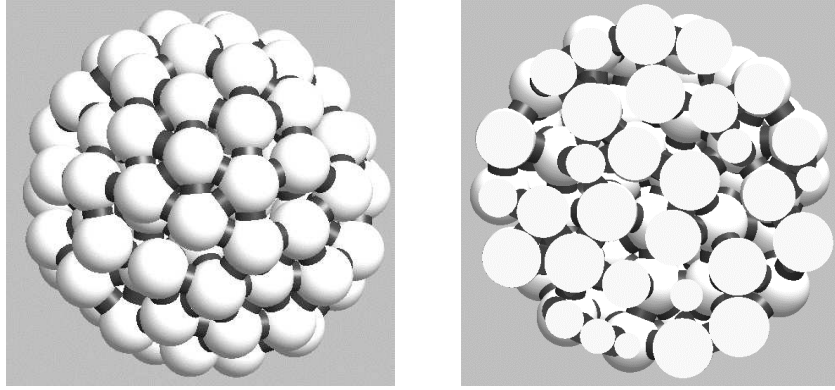
Figure 15. Dissipated energy during cyclic loadings (the same tests as of Figure 13).

Figure 16. Compressive curves of 20 loading-unloading cycles under  $0.1 \text{ mm/s}$  loading rate.

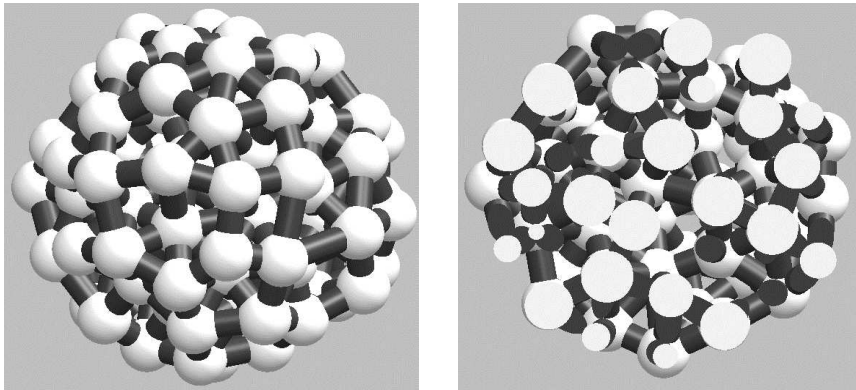
Figure 17. Energy loss coefficients of 20 loading-unloading cycles under  $0.1 \text{ mm/s}$  loading rate (the same tests as of Figure 16).

Figure 18. High speed camera recordings of impact test-rigid material bonded agglomerate.

Figure 19. High speed camera recordings of impact test-soft material bonded agglomerate.



(a) Dense structure (Porosity  $\varepsilon=44\%$  Coordination number CN=4.1)



(b) Loose structure ( $\varepsilon=57\%$  Coordination number CN=4.9)

Figure 1. Agglomerate structures (Left: front view Right: cross-sectional view).

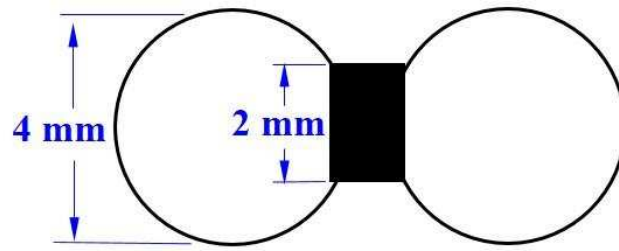


Figure 2. Schematic of a single doublet, the centre to centre distance between the particles varies based on the agglomerate design and for each particle.

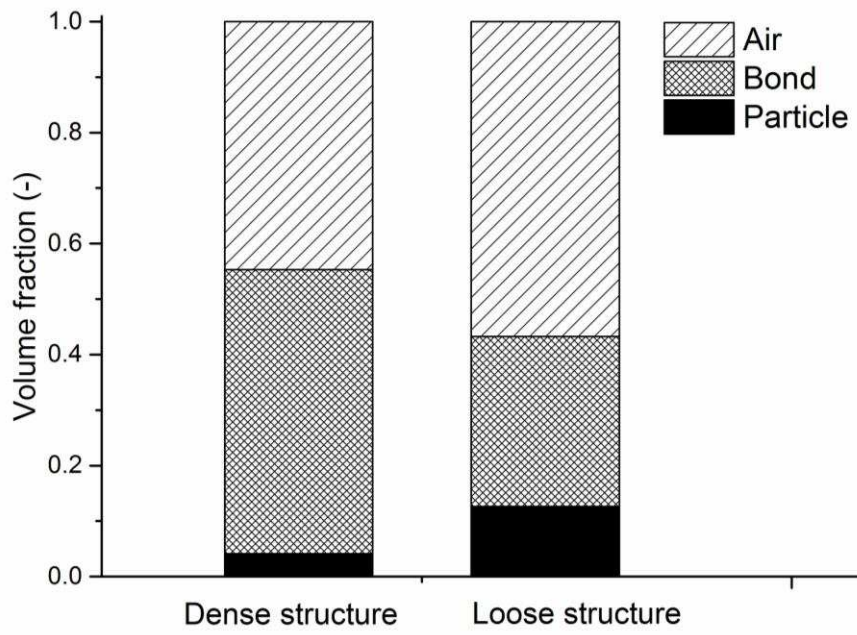
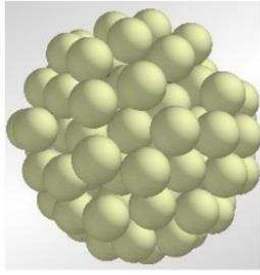
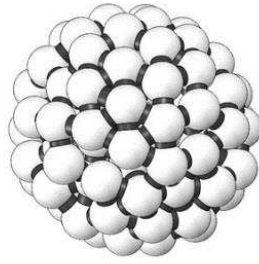


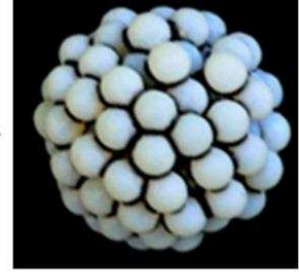
Figure 3. Phase volume fractions in two different agglomerate structures.



Create agglomerate by  
EDEM particle factory



Replicate agglomerate  
by Solidworks



3D Printed  
agglomerate

Figure 4. Agglomerate design and production process.

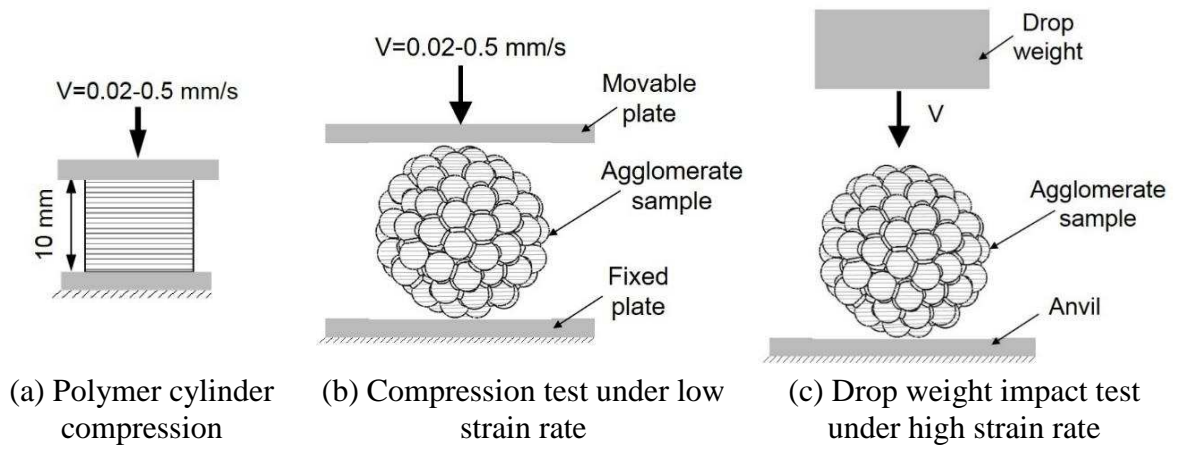
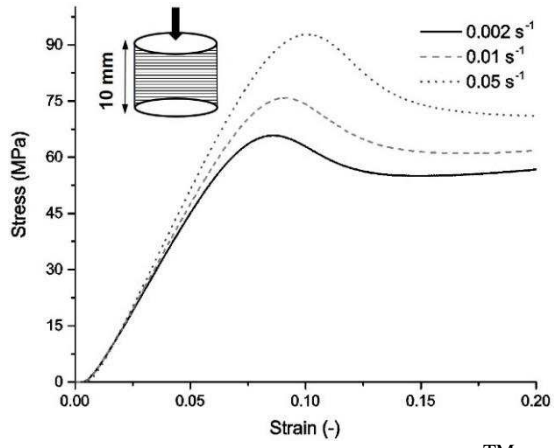
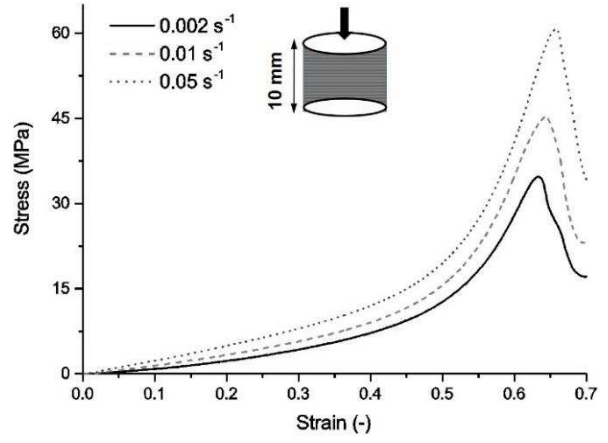


Figure 5. Schematic of breakage test setup.

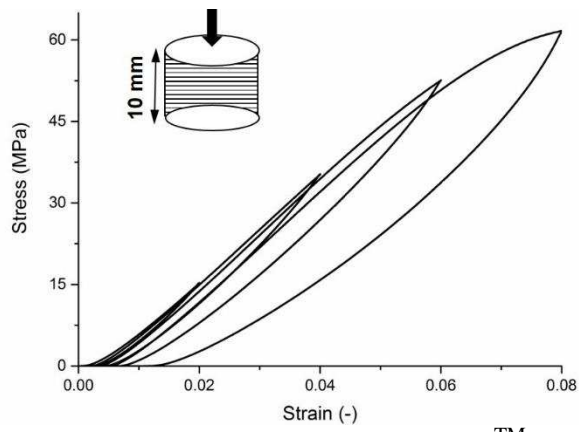


(a) Rigid material (Vero WhitePlus™)

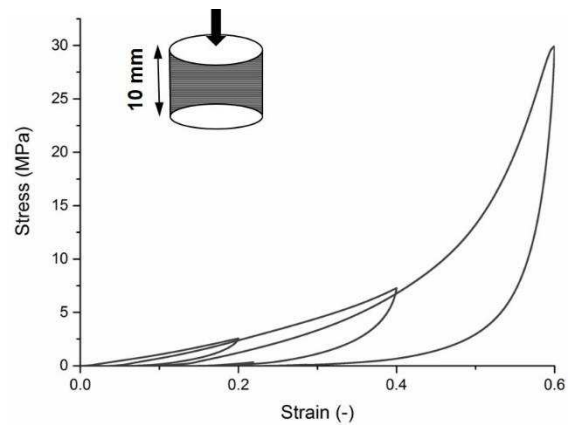


(b) Soft material (DM 9895)

Figure 6. Uniaxial compression curves of 3D printing materials.



(a) Rigid material (Vero WhitePlus™)



(b) Soft material (DM 9895)

Figure 7. Cyclic loading test results of 3D printing materials ( $0.002 \text{ s}^{-1}$  strain rate).

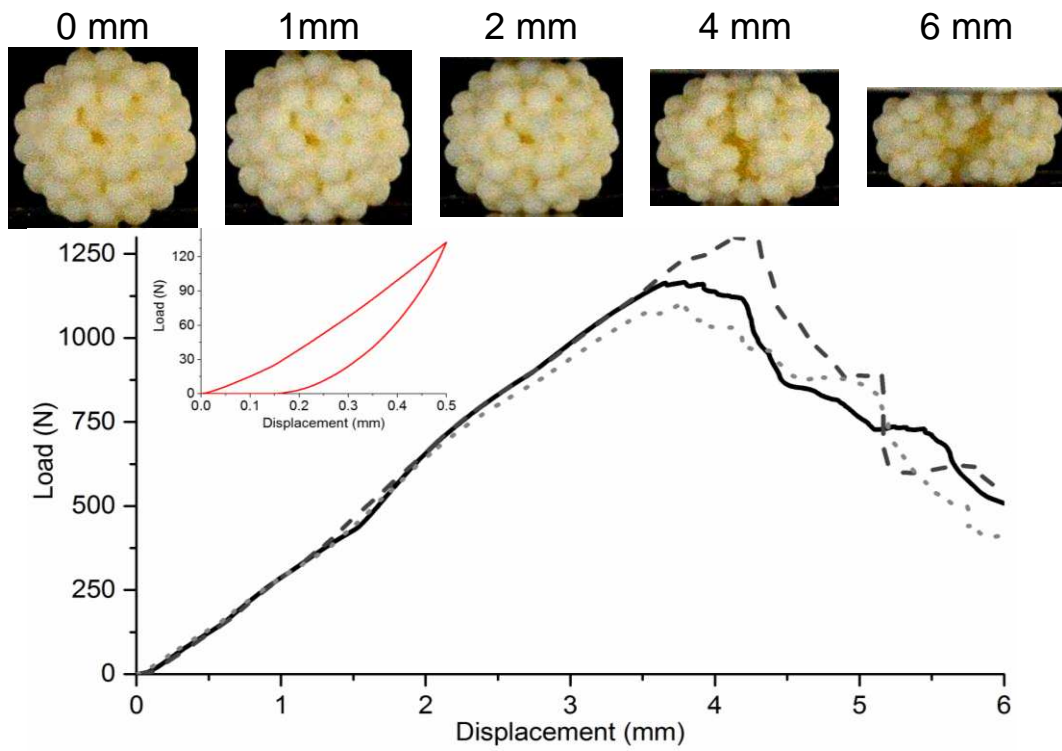


Figure 8. Force-displacement curves for the agglomerate with dense structure and rigid bond material under 0.02 mm/s loading condition (three replicates were performed, and a cyclic loading curve is shown in the inset).

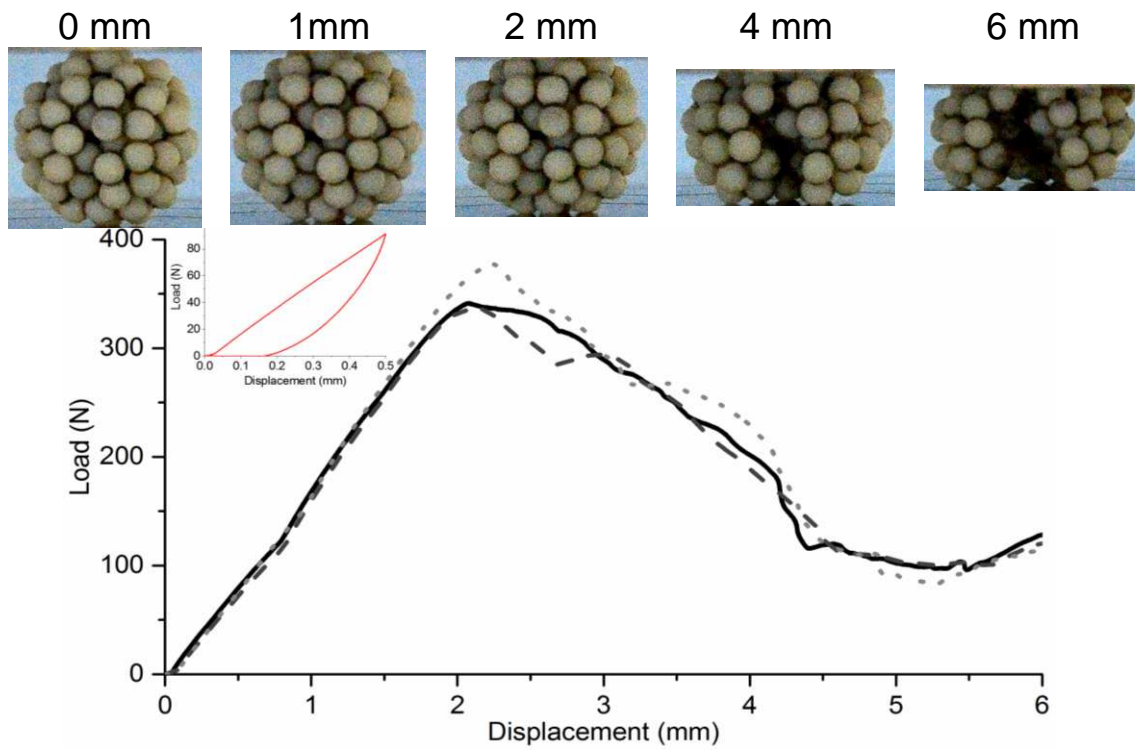


Figure 9. Force-displacement curves for the agglomerate with dense structure and soft bond material under 0.02 mm/s loading condition (three replicates were performed, and a cyclic loading curve is shown in the inset).

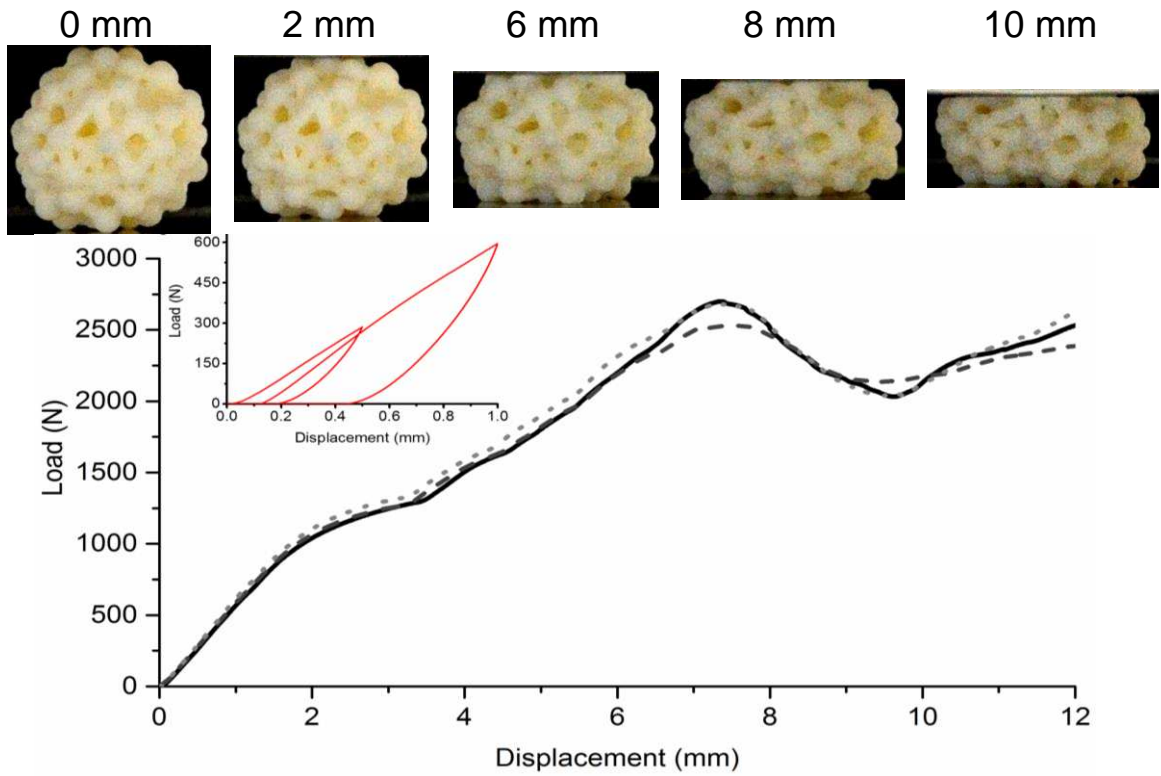


Figure 10. Force-displacement curves for the agglomerate with loose structure and rigid bond material under 0.02 mm/s loading condition (three replicates were performed, and a cyclic loading curve is shown in the inset).

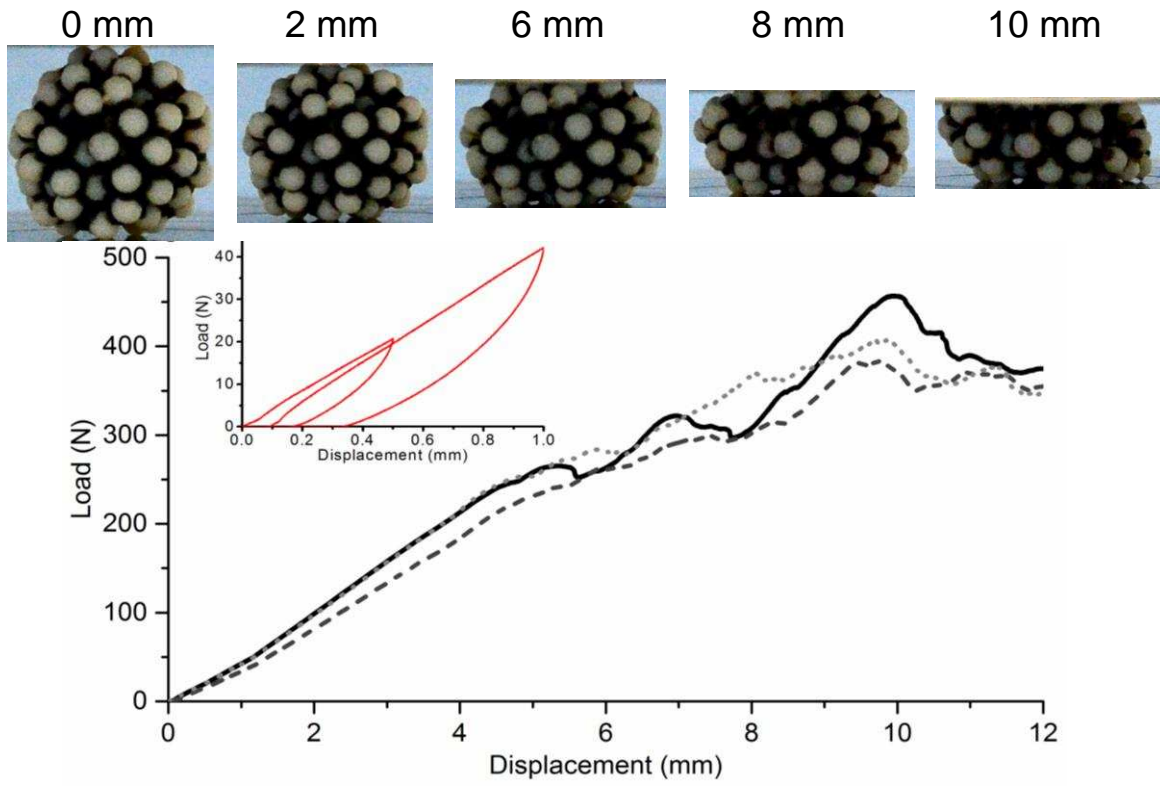
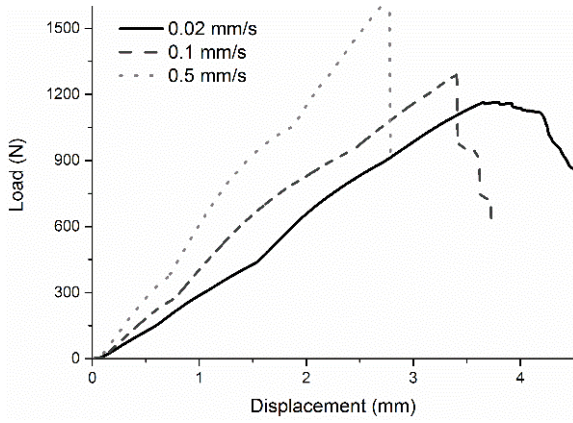
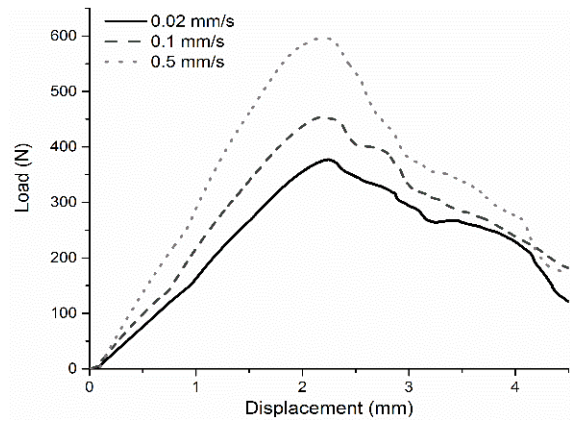


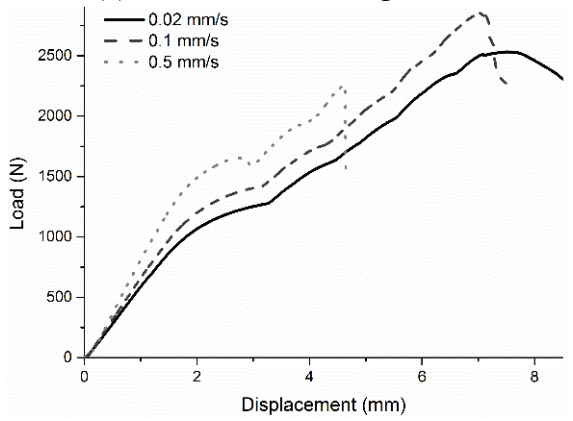
Figure 11. Force-displacement curves for the agglomerate with loose structure and soft bond material under 0.02 mm/s loading condition (three replicates were performed, and a cyclic loading curve is shown in the inset).



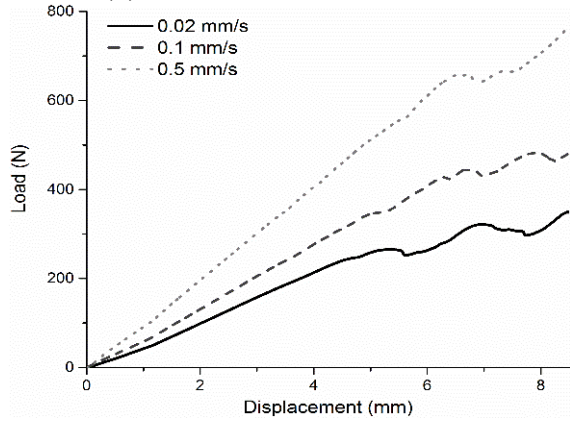
(a) Dense structure-Rigid bond



(b) Dense structure-Soft bond



(c) Loose structure-Rigid bond



(d) Loose structure-Soft bond

Figure 12. Force-displacement curves of various agglomerates under different loading conditions.

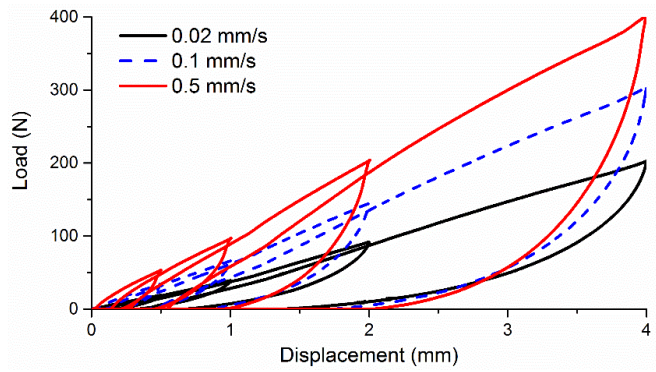
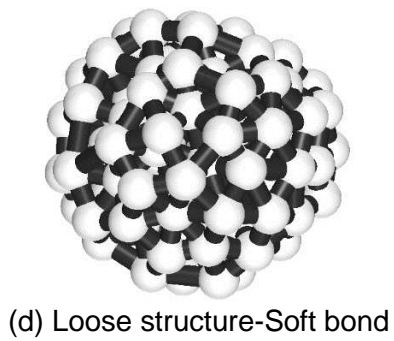
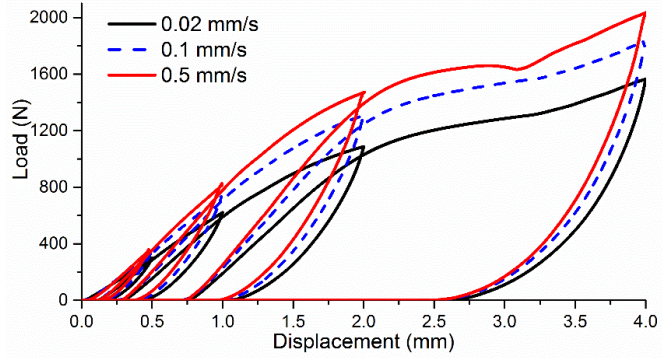
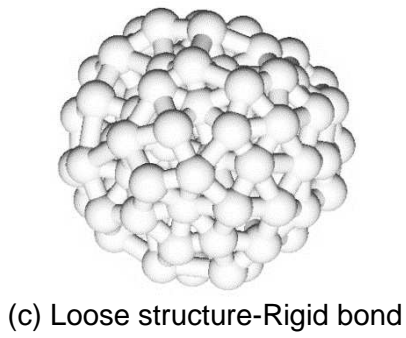
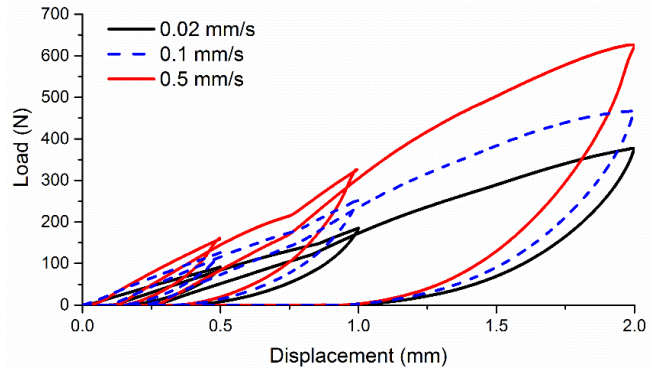
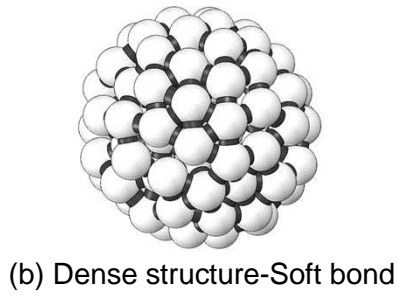
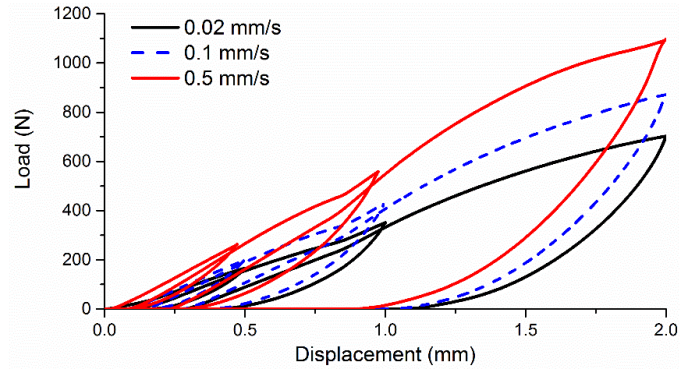
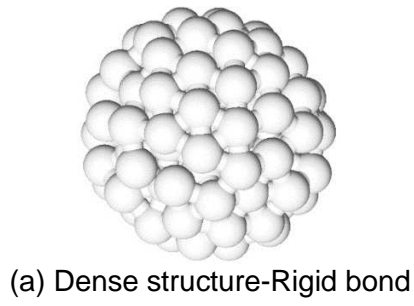


Figure 13. Compressive curves during loading-unloading cycles in sequence of increasing displacements.

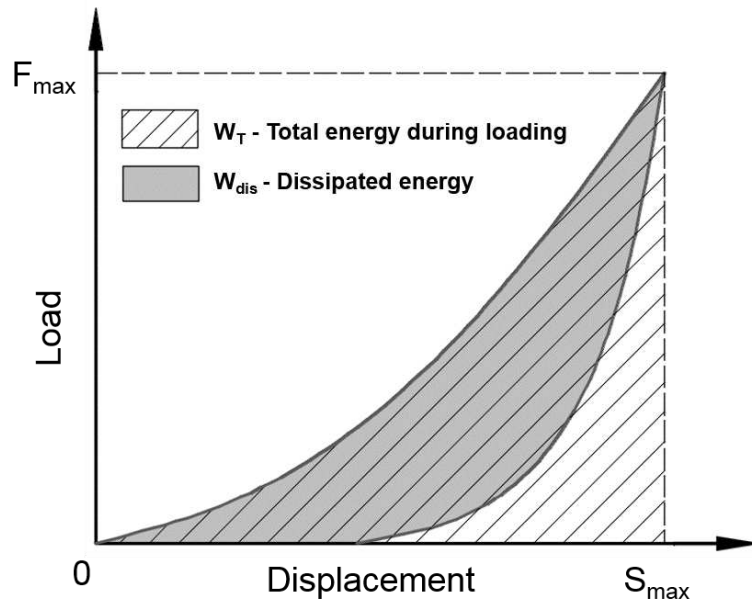
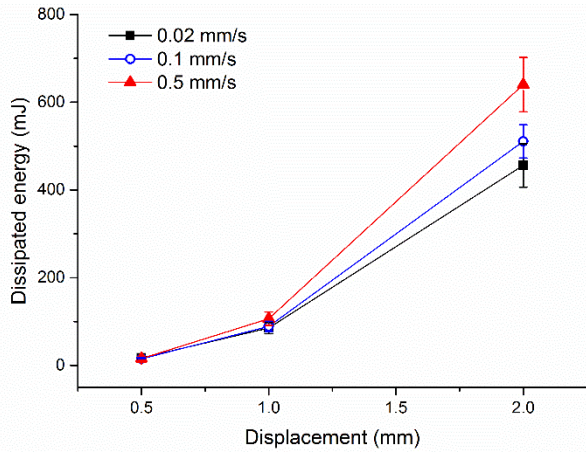
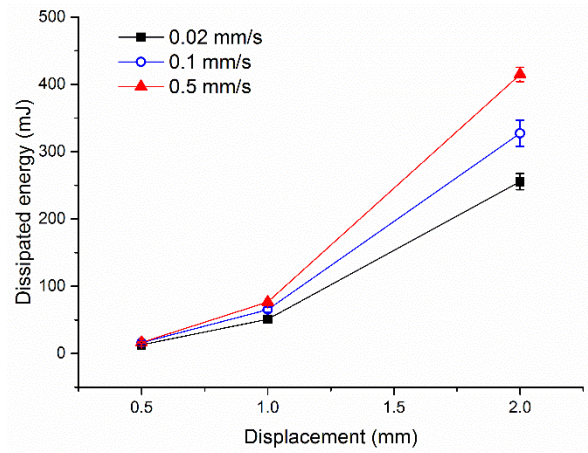


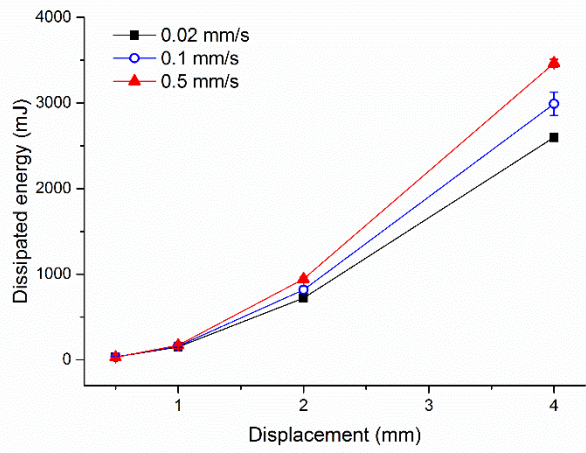
Figure 14. Schematic of dissipated energy.



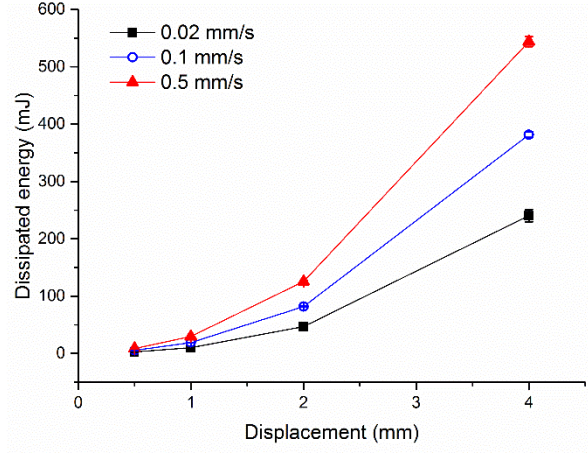
(a) Dense structure-Rigid bond



(b) Dense structure-Soft bond

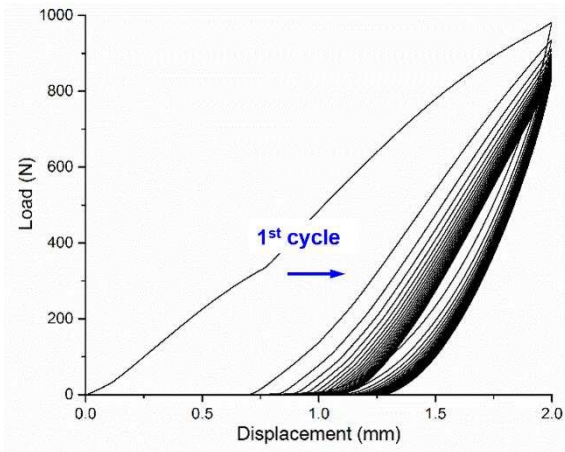


(c) Loose structure-Rigid bond

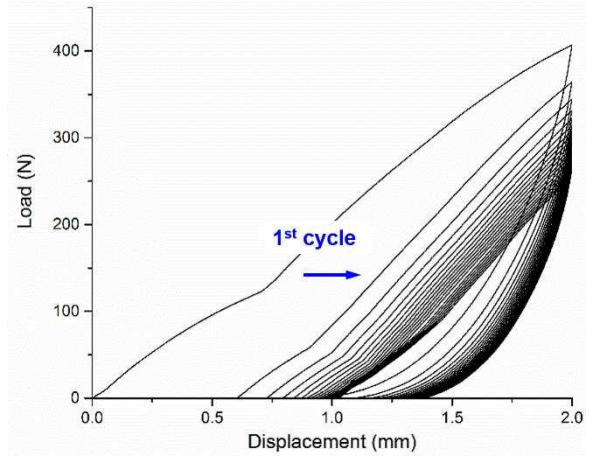


(d) Loose structure-Soft bond

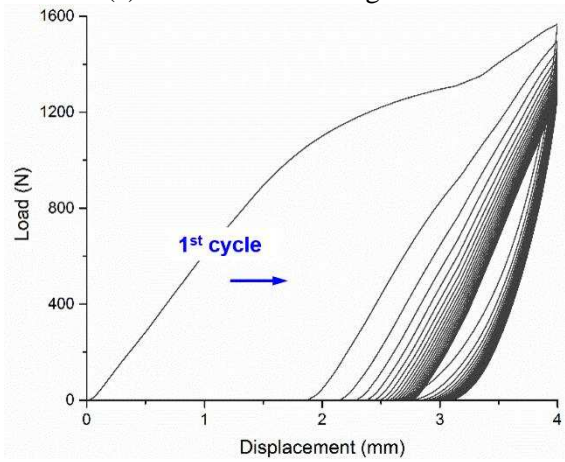
Figure 15. Dissipated energy during cyclic loadings (the same tests as of Figure 13).



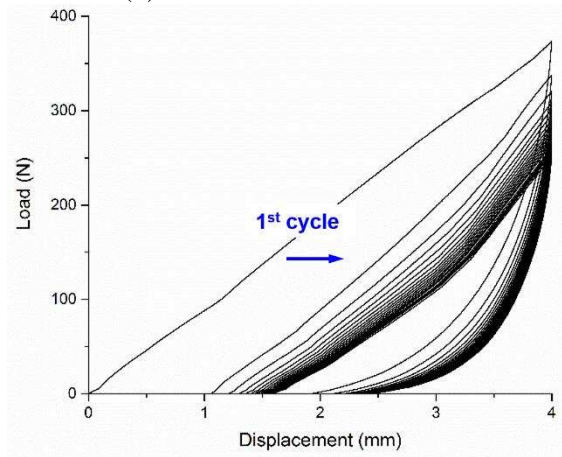
(a) Dense structure-Rigid bond



(b) Dense structure-Soft bond

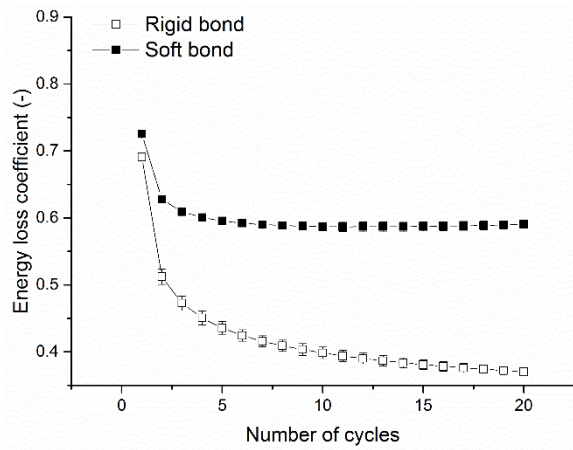


(c) Loose structure-Rigid bond

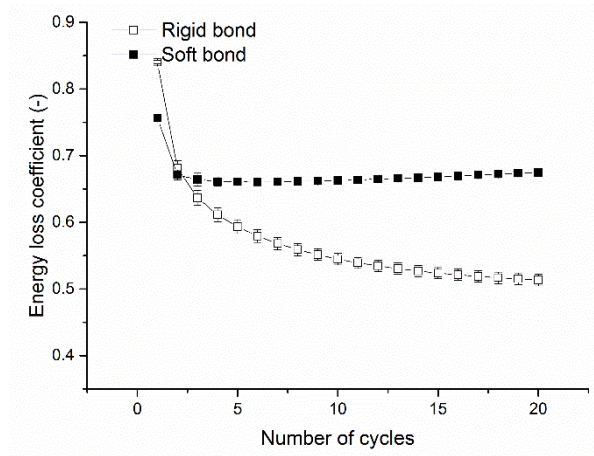


(d) Loose structure-Soft bond

Figure 16. Compressive curves of 20 loading-unloading cycles under 0.1 mm/s loading rate, the blue arrow indicates the direction of increasing cycle number.

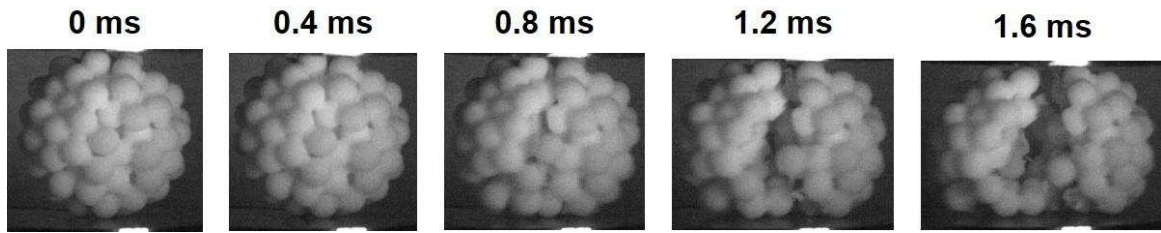


(a) Dense structure

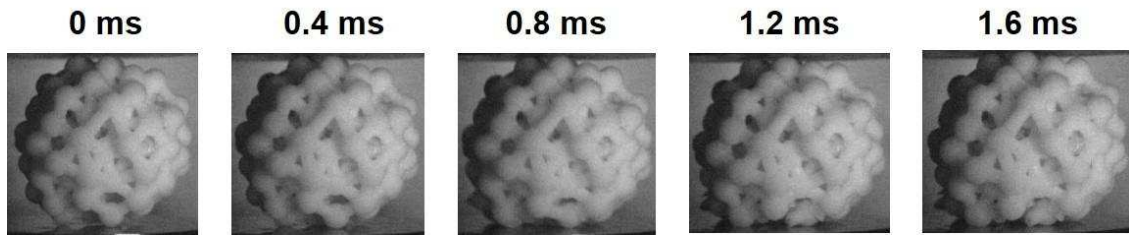


(b) Loose structure

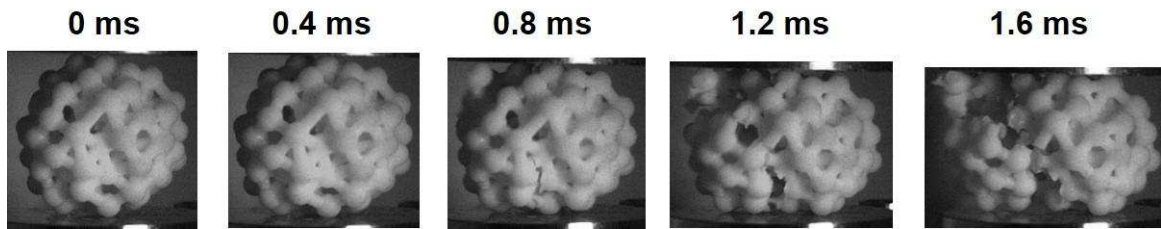
Figure 17. Energy loss coefficients of 20 loading-unloading cycles under 0.1 mm/s loading rate (the same tests as of Figure 16).



(a) Dense structure-Rigid bond, 0.9 J impact energy

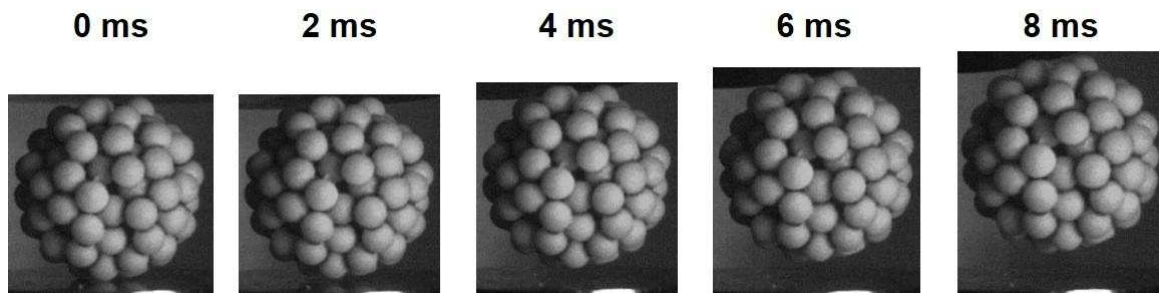


(b) Loose structure-Rigid bond, 0.9 J impact energy

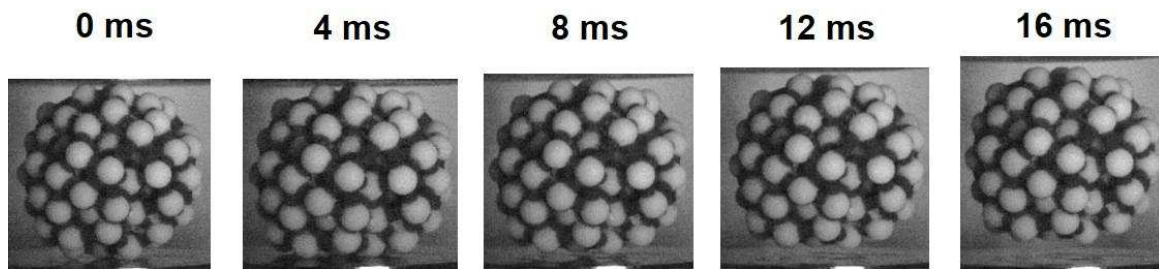


(c) Loose structure-Rigid bond, 2.7 J impact energy

Figure 18. High speed camera recordings of impact test-rigid material bonded agglomerate.



(b) Dense structure-Soft bond, 0.9 J impact energy



(e) Loose structure-Soft bond, 2.7 J impact energy

Figure 19. High speed camera recordings of impact test-soft material bonded agglomerate.

**Tables:**

Table 1. Agglomerate breakage studies using quasi-static compression test.

Table 2. Agglomerate breakage studies using impact test.

Table 3. Summary of four agglomerate types used in this research.

Table 4. Mechanical properties of rigid 3D printing materials (Vero WhitePlus™) under uniaxial compression tests, as a function of strain rate.

Table 5. Mechanical properties of soft 3D printing materials (DM 9895) under uniaxial compression tests, as a function of strain rate.

Table 2. Agglomerate breakage studies using quasi-static compression test.

<b>Authors</b>	<b>Agglomerate material</b>	<b>Size-fraction</b>	<b>Loading condition</b>
Meissner et al. [2]	Zinc oxide agglomerates	0.5-1 mm	-
Beekman et al.[3]	Enzyme based granules	500 $\mu\text{m}$	-
Sheng et al. [4]	Alumina particle based agglomerate (Polymeric binder)	180-250 $\mu\text{m}$	1-10 $\mu\text{m/s}$
Samimi et al. [5]	Detergent based granules	1-2 mm	0.1-0.5 mm/min
Antonyuk et al. [6]	$\text{Al}_2\text{O}_3$ agglomerate, Sodium benzoate	0.8-2 mm	0.02-0.15 mm/s
Cheong et al. [7]	Binderless polystyrene granule	3.35-4 mm	0.01-10 mm/min
Adi et al. [8]	Mannitol agglomerate	1.5 mm	1 mm/min
Russell et al. [9]	Zeolite 4AK granule (Solid mineral binder)	1.25-4 mm	0.01-0.15 mm/s

Table 2. Agglomerate breakage studies using impact test.

<b>Authors</b>	<b>Agglomerate type</b>	<b>Size-fraction</b>	<b>Loading condition</b>
Ning et al. [10]	Lactose agglomerates	250-355 $\mu\text{m}$	1-10 m/s
Subero et al. [11]	Glass ballotini bonded by epoxy resin	30 mm	2-8 m/s
Samimi et al. [12, 13]	Detergent based agglomerates	1 mm	5-40 m/s
Salman et al. [14]	Dry binderless granule	2-8 mm	2-20 m/s
Antonyuk et al. [15]	Al <sub>2</sub> O <sub>3</sub> agglomerate, Kostrolith, Sodium benzoate	0.8-2 mm	20-55 m/s
Khanal et al. [16]	Concrete agglomerates	150 mm	6-53 m/s

Table 3. Summary of four agglomerate types used in this research.

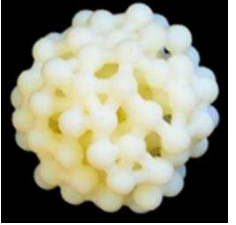
Densely packed structure ( $\epsilon=44\%$ , CN=4.1)		Loosely packed structure ( $\epsilon=57\%$ , CN=4.9)	
Rigid particles & rigid bonds (Vero WhitePlus™)	Rigid particles (Vero WhitePlus™) & Soft bonds (DM 9895)	Rigid particles & rigid bonds (Vero WhitePlus™)	Rigid particles (Vero WhitePlus™) & Soft bonds (DM 9895)
			
Dense structure Rigid bond	Dense structure Soft bond	Loose structure Rigid bond	Loose structure Soft bond

Table 4. Mechanical properties of rigid 3D printing materials (Vero WhitePlus™) under uniaxial compression tests, as a function of strain rate.

<b>Rigid material</b> <b>(Vero WhitePlus™)</b>	<b>Strain rate</b>		
	<b>0.002 s<sup>-1</sup></b>	<b>0.01 s<sup>-1</sup></b>	<b>0.05 s<sup>-1</sup></b>
Young's modulus (MPa)	1078.7±26.7	1139±28.9	1224±29.1
Failure strength (MPa)	68.4±2.2	77.3±3.2	90.2±4.1

Table 5. Mechanical properties of soft 3D printing materials (DM 9895) under uniaxial compression tests, as a function of strain rate.

<b>Soft material (DM 9895)</b>	<b>Strain rate</b>		
	<b>0.002 s<sup>-1</sup></b>	<b>0.01 s<sup>-1</sup></b>	<b>0.05 s<sup>-1</sup></b>
Young's modulus (MPa)	16.7±0.62	20.8±0.57	27.9±0.46
Failure strength (MPa)	34.1±1.8	47.2±3.6	59.3±4.9